Remaining Useful Life Prediction of Lithium-ion Batteries with Limited Degradation History Using Random Forest

Niankai Yang, Heath Hofmann, *Fellow, IEEE*, Jing Sun, *Fellow, IEEE*, and Ziyou Song, *Senior Member, IEEE*

***Abstract*—Predicting the remaining useful life (RUL) of a lithium-ion battery with its limited degradation history is critical as it ensures timely maintenance of electric vehicles and efficient reuse of second-life batteries. Considering realistic battery operating conditions, this work investigates the RUL prediction under partial charge and discharge with a limited degradation history of the target cell. Given its ability to inform feature importance, the random forest is adopted to help prioritize different battery measurements and identify the least amount of operating data required for accurate RUL prediction. By examining the prediction performance using one complete charge and discharge cycle, it is shown that the duration, used capacity, and voltage signals of both charge and discharge contain important features related to battery RUL. The prediction performance under partial charge and discharge is also studied under state-of-charge (SOC) uncertainties, revealing satisfactory performance achieved with the data collected over the SOC range of $[0.2, 0.8]$. Comparison with an existing convolutional neural network-based approach that uses four complete charge and discharge cycles verifies the enhanced onboard feasibility of the proposed approach. Sensitivity analysis against SOC ranges shows that the data in the SOC range of $[0.1, 0.2]$ contain the richest RUL-related information for lithium iron phosphate cells. Extensive validation on cells with different chemistry, ambient temperatures, and C rates further demonstrates the robustness of the proposed approach.**

***Index Terms*—Remaining useful life, Lithium-ion battery cells, Random forest, Partial charge and discharge**

NOMENCLATURE

μ_x	Various statistical features: mean ($x = 1$), variance ($x = 2$), skewness ($x = 3$), kurtosis ($x = 4$), minimum (μ_0), and maximum ($\bar{\mu}_0$)
C_x	Nominal ($x = n$) and actual ($x = a$) capacity of the cell [Ah].
N_x	Number of aging cycles to the present cycle ($x = p$) and end of life ($x = EOL$).
Q_x	Used capacity during charge ($x = c$) and discharge ($x = d$) [Ah].
R	Internal resistance of the cell [Ω].
T_x	Temperature during charge ($x = c$) and discharge ($x = d$) [$^\circ$C].
t_x	Duration for charge ($x = c$) and discharge ($x = d$) [min].
V_x	Voltage during charge ($x = c$) and discharge ($x = d$) [V].

This paper is based upon the work supported by the U.S. Office of Naval Research (ONR) under Grants N00014-16-1-3108 and N00014-18-2330 (Corresponding author: Ziyou Song.)

Niankai Yang and Jing Sun are with the Department of Naval Architecture and Marine Engineering, University of Michigan, Ann Arbor, MI 48109, USA. (e-mail: {ynk, jingsun}@umich.edu)

Heath Hofmann is with the Department of Electrical Engineering and Computer Science, University of Michigan, Ann Arbor, MI 48109, USA. (e-mail: hofmann@umich.edu)

Ziyou Song is now with the Department of Mechanical Engineering, National University of Singapore, Singapore 117575, Singapore. (e-mail: ziyou.songthu@gmail.com)

I. INTRODUCTION

Given their long lifetime and high energy density, lithium-ion batteries have been broadly used as power sources/energy storage systems nowadays for various applications, e.g., electric vehicles (EVs) [1], electronic devices [2], and microgrids [3]. To maintain reliability and cost-effectiveness of battery usage, one critical issue is to accurately predict the number of cycles till the end of useful life (EOL) of the lithium-ion batteries, also referred to as battery remaining useful life (RUL) prediction [4]. For example, in EV applications, the EOL is typically defined as the time when batteries degrade to 80% of the nominal capacity to ensure daily driving demand [5], and the RUL information can help to determine a proper and timely maintenance schedule for the vehicle [6]. In renewable energy systems, second-life batteries are widely deployed, where RUL information will be important to assess the economic benefit of using these batteries [7].

While a profound understanding of the battery degradation mechanism has been established [8], it remains challenging to accurately predict the RUL of batteries in real applications, which might be primarily due to the following reasons. First, as an electro-chemical system [9], the degradation of lithium-ion batteries is an interplay of various complex phenomena influenced by the operating condition (e.g., C rates and ambient temperature) [10]. Consequently, its dynamics can be highly nonlinear and subject to the impact of multiple inputs. Second, in most practical applications, only limited degradation data (or history) of the target cell can be collected/stored online for its RUL prediction due to operational constraints. For instance, operating data in low or high state of charge (SOC) regions may be unavailable due to partial charge/discharge [11]. Only the data of the present cycle/the last few cycles may be accessible with stringent onboard memory constraints [12], e.g., smartphones and second-life batteries. As a result, the richness of RUL-related information in the data can decrease significantly, leading to a more demanding RUL prediction problem.

To tackle the RUL prediction of batteries, early works focus on developing model-based approaches. The model-based approaches typically achieve the RUL prediction in two stages. During the offline stage, the structure of a physics/empirical-based degradation model is first established. The model parameters are then identified during the online stage based on the operating data of the target cell to provide the RUL prediction for the cell [13]. For example, in [14], a two-term logarithmic model was developed to capture the degradation trends of batteries for predicting RUL. The battery degradation rate was modeled by the Wiener process in [15] to account for stochasticity under different temperature conditions when predicting RUL. An Arrhenius law-based model was adopted in [16] to take the impact of discharge rate into consideration. Besides using different modeling approaches to better capture the underlying degradation dynamics, studies were also conducted with various parameter estimation approaches, e.g., Kalman filter [17], unscented Kalman filter [18], and particle filter [19], to improve the RUL prediction accuracy of model-based approaches. The model-based approaches can be efficiently implemented with low memory and computational overhead. Nevertheless, the degradation model can still be oversimplified to capture the thermal, electrical, and chemical interactions, leading to compromised performance.

With the advancement in data-driven modeling approaches and the increasing data availability, machine learning approaches have become promising and alternative solutions for RUL prediction. Trained offline with the degradation data of similar cells, machine learning models are capable of predicting RUL after taking in the operating data of the target cell collected online [20]. For instance, the support vector machine was applied with a particle filter for simultaneously obtaining the state of health (SOH) and RUL of batteries in [21]. In [22], the random forest was integrated with a model-based approach to correct its RUL prediction error for enhanced accuracy. An artificial neural network was used in [23] to leverage the strong learning ability of deep learning approaches for RUL prediction. To consider the temporal dependency in the RUL prediction, recurrent neural networks such as long-short term memory networks and gated recurrent units were also studied in [24], [25]. Being model-free, machine learning approaches can learn the degradation dynamics from the data, well tackling the challenge of complex degradation dynamics and achieving satisfactory RUL prediction accuracy. However, the challenge of limited degradation data availability for the target cell can frequently be overlooked in the aforementioned RUL prediction studies, which may impair the feasibility of proposed approaches or significantly degrade the performance in real-world applications.

In this paper, we focus on the RUL prediction problem where only limited degradation data/history of the target cell is available online for its RUL prediction. Recently, efforts to tackle this challenge have emerged in the literature. For example, the authors in [26] showed that the last four complete charge and discharge cycles are required to predict RUL accurately with a convolutional neural network (CNN). In [27], RUL prediction was achieved with one of the aging cycles within the first 100 cycles, and later work [28] further demonstrated that the first cycle might contain sufficient information for RUL prediction. Although these studies have considerably reduced the need for collecting and storing a long/entire degradation history of the target cell, obtaining early aging cycles or the last few cycles could still be prohibitive for some real-world applications (e.g., second-life batteries). Meanwhile, assuming data availability under complete charge and discharge can also make the proposed solution restrictive.

To bridge the gap of RUL prediction under limited degradation data/history, we aim to study the RUL prediction under partial charge and discharge while reducing the number of past cycles required for achieving satisfactory RUL prediction accuracy. To this end, the random forest technique is adopted [29], which produces a prediction by aggregating the predictions from multiple decision trees constructed with different combinations of the input features. When choosing these feature combinations during tree construction, the information gain or variance reduction is typically used as the criteria [30]. This information naturally implies the importance of different features, which can be directly leveraged to reduce the required degradation data without significantly deteriorating the RUL prediction accuracy. By applying random forest to an open-source dataset in [31], it is first shown that the duration, change in the charge, and voltage in the present charge and discharge cycles are critical for RUL prediction. The feasibility of RUL prediction under partial charge and discharge is then examined, which reveals that satisfactory RUL prediction can be achieved over a SOC range of $[0.2, 0.8]$. The effectiveness of the proposed approach is verified by comparing it to the CNN approach in [26]. Extensive validation on other open-source datasets further demonstrates its effectiveness under different temperatures, C rates, and cell chemistry.

The main contributions of this paper are given as follows.

- The importance of the RUL-related indicators in past cycles, different battery measurements (e.g., time, current, voltage, temperature, and internal resistance), and different SOC ranges are revealed.
- A novel RUL predictor is proposed using summary statistics from battery measurements and random forest as the regression algorithm.
- The RUL prediction performance under various realistic scenarios (e.g., different temperatures, C rates, cell chemistry, partial charge and discharge under uncertain SOC information) is quantified.

The above contributions could greatly enhance the feasibility of RUL prediction for applications with stringent operational requirements. Without these requirements, it could still help reduce data collection/storage efforts during the online application, thereby benefiting the algorithm efficiency.

The remainder of this paper is organized as follows: Section II introduces the adopted dataset with its processing procedure and formulates the RUL prediction problem. The random forest is then applied for RUL prediction with a complete charge and discharge cycle in Section III, followed by a feature importance analysis. In Section IV, RUL prediction performance of the proposed random forest approach under partial charge and discharge is studied. To verify the proposed approach, it is first compared with the RUL prediction ap-

proach in [26] in Section V, along with a sensitivity analysis of the prediction performance under different SOC intervals. Meanwhile, extensive validation on different temperatures, C rates, and cell chemistry is also conducted in this section. Finally, Section VI provides conclusions and future work.

II. Background

In this section, the dataset employed for the subsequent study is first presented. Then, the RUL definition is introduced, followed by the illustration of data processing. Finally, the RUL prediction problem under limited degradation data/history (of the target cell) is formulated.

For the model development and feature importance analysis purpose, we utilize the battery cell degradation dataset in [31], which contains 124 commercial lithium iron phosphate (LFP)/graphite cells manufactured by A123 Systems (model APR18650M1A). This specific dataset is adopted due to the following reasons. First, most cells are sufficiently aged for studying RUL prediction in many real applications (e.g., reached 80% nominal capacity for an EV case study). Second, it contains the degradation data of a sufficient number of cells to ensure the statistical significance of the results and demonstrate the robustness of the proposed approach, e.g., prediction performance under cell-to-cell variations.

In the dataset, the nominal capacity of the cell is 1.1 Ah, and the low and high cutoff voltages are 2.0 V and 3.6 V, respectively. To age the cells, the cells are cycled repeatedly in a temperature-controlled chamber at a constant temperature of 30 C. All cells were cycled with the same discharge profile, a constant 4 C discharge to the low cutoff voltage with a taper current of $1/50$ C. The charge profile varies across cells. Different multi-step fast charge profiles were adopted to charge the cell from 0% to 80% SOC within 9 to 13.3 minutes. All cells were then charged to 100% SOC at 1 C with a taper current of $1/50$ C. During each aging cycle (including a charge and a discharge cycle), the cell surface temperature, current, and terminal voltage were measured over time. In addition, one internal resistance value was obtained for each aging cycle by utilizing 10 pulses with an amplitude of ± 3.6 C and a pulse width of 30 to 33 ms conducted at 80% SOC during the charging process. See [31] for more details.

Since the operating condition remains the same for each cell in the adopted dataset, in this study, we consider the RUL prediction problem for cells undergoing identical aging cycles throughout their entire life. This problem is important as many applications have nearly identical load profiles. One aging cycle is then defined as a repetition of the operation/load profile (e.g., one charge and discharge cycle in the adopted dataset). For each aging cycle, we first define the SOH of a cell as follows:

$$SOH = \frac{C_a}{C_n}, \tag{1}$$

where C_n is the nominal capacity of a cell, and C_a is the actual capacity of the cell at the present cycle, defined as the maximum discharge capacity.

We assume a cell reaches its EOL when its SOH is reduced to 0.8 (see Fig. 1), as is the general practice in the EV industry [32]. We point out that the SOH value corresponding to EOL can vary with the application (e.g., for second-life batteries [33]). Let us denote the number of aging cycles to reach EOL as N_{EOL}. The RUL of a cell at the p^{th} aging cycle from the first cycle is then computed as

$$N^p_{RUL} = N_{EOL} - N_p, \tag{2}$$

where N_p is the number of aging cycles accumulated from the first cycle to the present cycle. A graphical illustration of the RUL definition is also provided in Fig. 1.

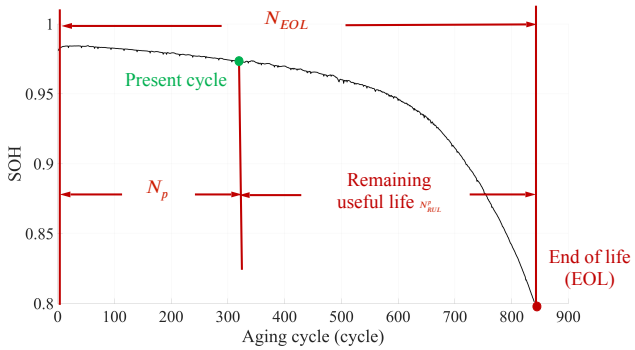

Fig. 1: Illustration of the RUL definition of a cell at its p^{th} aging cycle (the black line is the cell SOH trajectory over cycles)

Based on the above definitions, the SOH trajectory and the number of cycles to EOL of each cell in the dataset of [31] are provided in Fig. 2. As shown in Fig. 2a, most cells undergo first linear and then nonlinear aging stages [34]. In the latter stage, the EOL is quickly approached as the cells begin to have rapid degradation caused by lithium plating. In addition, the cells exhibit different aging patterns, namely, the cycles where the knee point appears can differ substantially [35]. Finally, there is also a high variance in the cell cycle life ranging from nearly 300 to 2000, as can be seen in Fig. 2b. The above observations verify that the adopted dataset contains sufficient cell-to-cell variations to well showcase the robustness of the proposed approach.

To process the dataset for the RUL study, the RUL is computed using (2) for each aging cycle. For each cell, there are N_{EOL} RUL prediction instances (i.e., from the first to the last aging cycle) throughout its cycle life. In this study, we will then tackle the RUL prediction for a battery cell throughout its cycle life. Meanwhile, we aim at reducing the required degradation data/history of the target cell for its RUL prediction, thereby facilitating its application in real-world applications.

III. RUL prediction under complete charge & discharge

In this section, the details of the available data (i.e., measurements) of the target cell in each aging cycle are first shown, followed by presenting the adopted summary statistics to extract features from the available data for RUL prediction. Next, the methodology of random forest for RUL prediction and feature importance analysis is introduced. Finally, we

This article has been accepted for publication in IEEE Transactions on Transportation Electrification. This is the author's version which has not been fully edited and content may change prior to final publication. Citation information: DOI 10.1109/TTE.2023.3323976

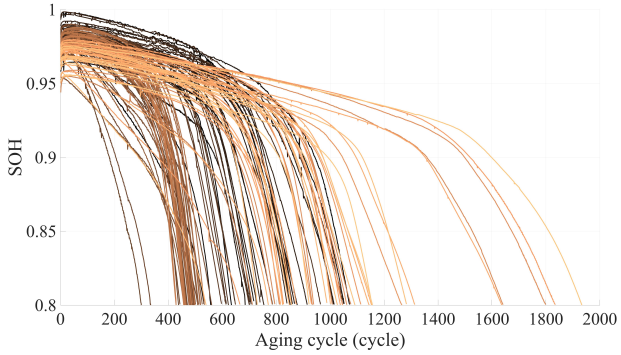

(a) SOH trajectories of all cells (each color indicates one cell)

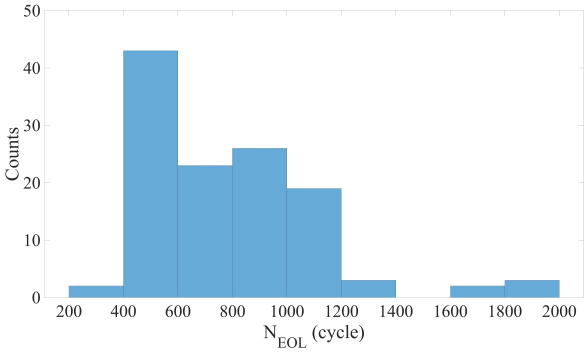

(b) Histogram of the cycles to reach EOL of all cells

Fig. 2: Degradation data for all cells that reach the EOL from the dataset in [31]

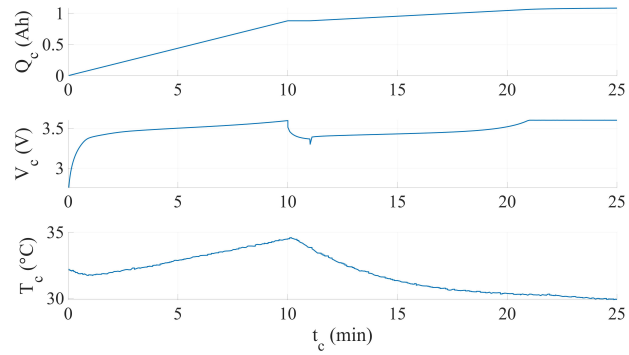

(a) Charge data

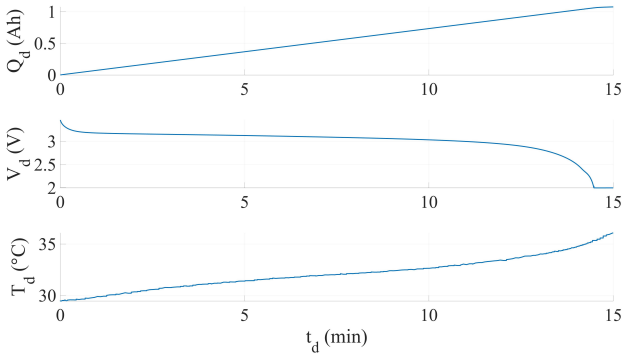

(b) Discharge data

Fig. 3: Temperature, voltage, and change in the charge (i.e., used capacity) signals of one aging cycle from the dataset in [31]

examine the performance of random forest models using the available data in the present aging cycle and discuss the importance of different features in RUL prediction.

A. Degradation data and RUL features

In each aging cycle, the internal resistance (R), charge & discharge time (t_c & t_d), charge & discharge temperature (T_c & T_d), charge & discharge used capacity (Q_c & Q_d), and charge & discharge voltage (V_c & V_d) are collected, which may all contain RUL-related indicators. As is discussed in Section II, the internal resistance is a scalar value for each cycle obtained during charging at 80% SOC. The charge/discharge time counts from zero as the battery starts to charge/discharge. The change in the charge (i.e., used capacity) during charge & discharge is considered instead of current since the used capacity contains important information to infer the battery SOH (even under partial cycles) [36], [37]. The time, temperature, change in the charge, and voltage sequences during charge & discharge are illustrated in Fig. 3.

Considering that the data available for RUL prediction contains scalars and vectors, one may concatenate all the scalars and vectors as an augmented input vector to be fed into the random forest model. However, this will result in an excessively large computation overhead and huge input size, making the key features less distinguishable. Instead, we engineer features from the sequences in this study by adopting the summary statistics, which can provide a powerful synthesis of distributions/time series [38]. Let us denote a real-valued random variable (e.g., t, T, Q, and V) as X. We consider the following summary statistics:

- Mean (μ_1): first central moment describing the central tendency of the variable X;
- Minimum ($\underline{\mu}_0$) & maximum ($\bar{\mu}_0$): extreme values of the variable X;
- Variance (μ_2): second central moment describing the statistical dispersion of the variable X;
- Skewness (μ_3) & kurtosis (μ_4): third and fourth central moments describing the shape of the distribution of the variable X, computed as

$$\mu_i = \mathbb{E}\left[\left(\frac{X-\mu_1}{\sqrt{\mu_2}}\right)^i\right], \text{ for } i = 3, 4, \tag{3}$$

  where $\mathbb{E}(\cdot)$ is the expectation operator.

Based on the adopted summary statistics, (all or part of) the features listed below will be the inputs to the random forest models investigated in the subsequent sections:

- Internal resistance (R);
- Mean ($\mu_1^{t_j}$), max ($\bar{\mu}_0^{t_j}$), variance ($\mu_2^{t_j}$), skewness ($\mu_3^{t_j}$), and kurtosis ($\mu_4^{t_j}$) of t_j;
- Mean ($\mu_1^{V_j}$), variance ($\mu_2^{V_j}$), skewness ($\mu_3^{V_j}$), and kurtosis ($\mu_4^{V_j}$) of V_j;
- Mean ($\mu_1^{Q_j}$), max ($\bar{\mu}_0^{Q_j}$), variance ($\mu_2^{Q_j}$), skewness ($\mu_3^{Q_j}$), and kurtosis ($\mu_4^{Q_j}$) of Q_j;

- Min ($\underline{\mu}_0^{T_j}$), max ($\bar{\mu}_0^{T_j}$), mean ($\mu_1^{T_j}$), variance ($\mu_2^{T_j}$), skewness ($\mu_3^{T_j}$), and kurtosis ($\mu_4^{T_j}$) of T_j,

where $j = c/d$ denotes the features from the data collected in the charge/discharge cycle, respectively. The minimum time and used capacity during charge & discharge are not included, as they are always zero. The minimum and maximum terminal voltages are also not included, as they are typically close to the low- and high-cutoff voltage and provide limited useful information.

B. Random forest technique

The random forest is an ensemble learning method built upon a combination of decision trees. A single decision tree easily overfits the training data while lacking generalizability to the unseen data. Unlike decision trees, the random forest synthesizes the outputs from a collection of decision trees (e.g., by averaging or majority votes), thereby mitigating the overfitting issue [39]. More importantly, random forest is a well-known feature selector. As discussed in the introduction, the inherent structure of the random forest (or decision tree) permits good interpretability of the importance of the input features to the model. This information can then be used to assess the redundancy in the inputs and facilitate relaxing the need for degradation data.

In this work, the random forest models are set to take in the statistical features extracted from the battery operating data (discussed in Section III-A) at the present cycle and output the RUL at the present cycle. The random forest model is developed in Scikit-learn [40]. The criterion to measure the quality of a split is the mean squared error (i.e., variance reduction), and 90% features are considered when looking for the best split. The maximum depth of each decision tree is 9, and 50 trees are considered in the random forest model. The above parameters were obtained by trial and error. The permutation-based feature importance [41] is adopted, which essentially measures the decrease in the prediction accuracy after randomly shuffling the features. Note that, considering that RUL prediction is a regression problem, impurity-based importance is not chosen to avoid potential robustness issues from high cardinality features.

The processed dataset for model development and evaluation consists of the statistical features extracted following the procedure presented in Section III-A and the RUL values computed with (2). The data for 60% of the cells are randomly selected for training. The data for 20% of the cells are randomly picked for validation, and the rest is used for testing. To remove performance biases caused by the dataset partition, we use different cells to form the validation set (resulting in five different dataset partitions) and select the partition that achieves the average performance among the five as the representative partition for the subsequent analysis (i.e., five-fold cross-validation). To evaluate performance, we adopt the following mean absolute error (MAE):

$$\text{MAE} = \frac{1}{N_t}\sum_{n=1}^{N_t}\frac{\sum_{p=1}^{N_{EOL,n}}|\hat{N}_{RUL,n}^{p} - \tilde{N}_{RUL,n}^{p}|}{N_{EOL,n}}, \quad (4)$$

where N_t is the number of cells in the testing data, $(\cdot)_n$ denotes the variable of the n^{th} cell, $\hat{(\cdot)}$ denotes the prediction, and $\tilde{(\cdot)}$ denotes the ground truth value. Since RUL prediction concerns how many cycles a user can use the battery before its EOL, the MAE can directly imply the prediction accuracy in cycles.

C. Performance evaluation and feature importance analysis

We first examine the prediction performance and feature importance by using all available information of one complete present aging cycle. A random forest model is developed to take in the R, t_j, T_j, Q_j, and V_j ($j = c, d$) features from the complete present aging cycle and output the RUL of the present cycle (i.e., model-a in Table I). The MAE of the RUL predictions is 62 cycles over the cells in the testing data. The RUL prediction and the absolute prediction error over aging cycles for the cells are also shown in Fig. 4. It can be seen that the random forest model can make reasonable RUL predictions, e.g., the predicted RUL decreases in general as the true RUL decreases. However, some information the random forest model-a requires can be hard to obtain in real-world applications (e.g., reliable temperature and resistance information) [42]. Therefore, feature importance analysis is performed with the random forest model-a to reveal the necessity of these inputs. The top ten most important features (among forty-one total features) are given in Fig. 5. The following observations can be made from Fig. 5.

Observation 1: The variance of the used capacity during discharge has the largest importance, indicating that the used capacity during discharge contains the most important feature for RUL prediction.

Observation 2: Among the top ten important features, the number of features from discharge data is the same as that from charge data, showing that both the charge and discharge data are important for RUL prediction.

Observation 3: Internal resistance and cell temperature-related features are ranked low in importance analysis. This implies that, in a temperature-controlled operating environment, the variations in the cell temperature and internal resistance may contain minimal RUL-related information.

Observation 1 is expected as the used capacity during discharge is closely related to the cell capacity that defines the EOL/RUL. Observation 2 is also reasonable since the RUL is affected by both the charge and discharge conditions. Observation 3 can be subject to the specific testing condition of the adopted dataset, i.e., in a temperature-controlled aging chamber. However, the ambient temperature will typically be controlled to stay near a pre-defined thermal setpoint in real-world applications for safe and efficient battery operations. Meanwhile, a model with a different nominal temperature can be developed and deployed in the case of a change in the battery thermal control setpoint. Finally, considering that thermal measurements usually contain high uncertainties, leaving out thermal information can be a reasonable practice. The internal resistance is correlated with the cell capacity [43]. However, its value can contain high uncertainties as the resistance estimation is subject to both current and voltage

This article has been accepted for publication in IEEE Transactions on Transportation Electrification. This is the author's version which has not been fully edited and content may change prior to final publication. Citation information: DOI 10.1109/TTE.2023.3323976

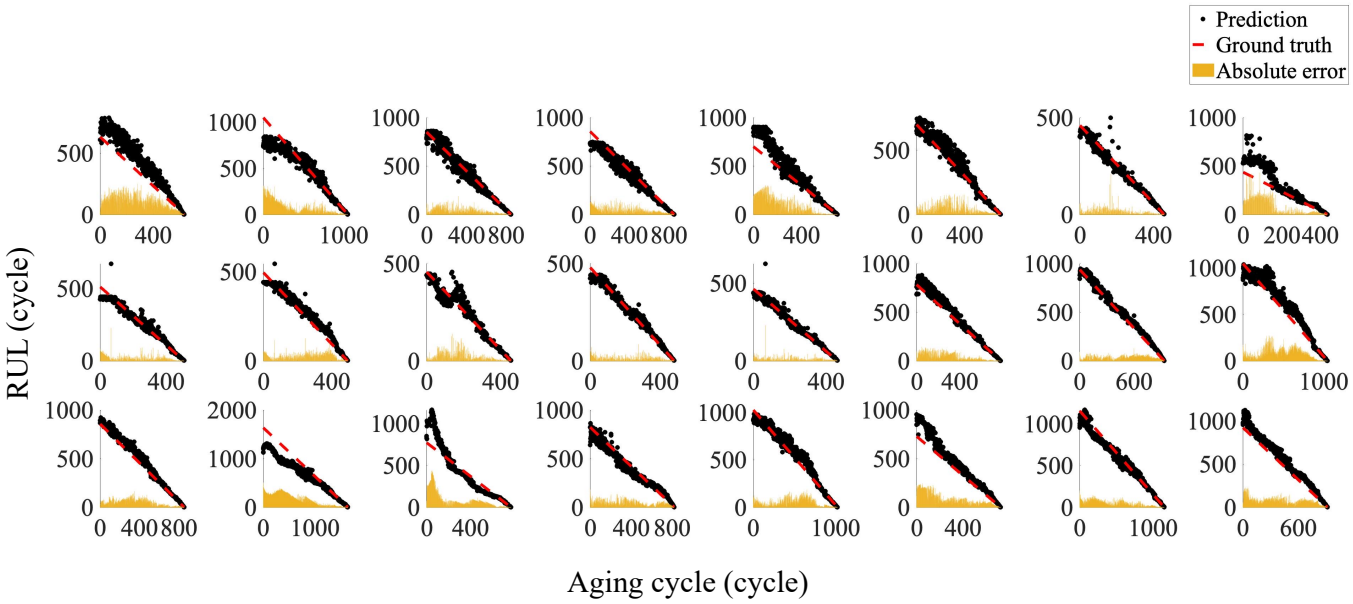

Fig. 4: RUL predictions, ground truth RUL values, and absolute RUL prediction error over aging cycles across the cells in the testing data from [31] under complete charge & discharge (model-a in Table I using features from $t_c, t_d, V_c, V_d, Q_c, Q_d, T_c, T_d, R$; each subplot contains the results for a different cell)

sensing noises, leading to a worse cell capacity estimate than the used capacity. Consequently, including internal resistance besides the used capacity may only gain marginal information.

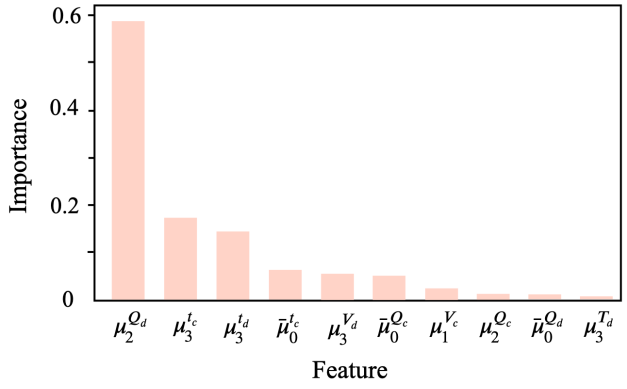

Fig. 5: Top ten important features from feature importance analysis of the random forest model-a in Table I

The relationships between the RUL, the variance of used capacity during discharge $\mu_2^{Q_d}$, the skewness of charge time $\mu_3^{t_c}$, the maximum used capacity during discharge $\bar{\mu}_0^{Q_d}$, and the internal resistance R are provided in Fig. 6 to further clarify the feature importance observed in Fig. 5. According to the correlation between RUL and extracted features in Fig. 6, cells in the dataset can be roughly categorized into three clusters, corresponding to the cells plotted in dark, medium, and light brown colors. While having a similar nonlinear relationship with RUL, the variance of used capacity during discharge (in Fig. 6a) has the most consistent relationship across the cells in each cluster compared to the maximum used capacity during discharge (in Fig. 6c) and the internal resistance (in Fig. 6d). Consequently, the variance of used capacity during discharge has a higher feature importance than the maximum used capacity during discharge and internal resistance. The skewness of charge time also has a high feature importance. This is because it has a different nonlinear relationship with RUL that could facilitate better differentiation of three clusters, as shown in Fig. 6b. The effectiveness of the skewness of charge time for distinguishing the three clusters might be due to the impact of the charge policies, which differs in the adopted dataset.

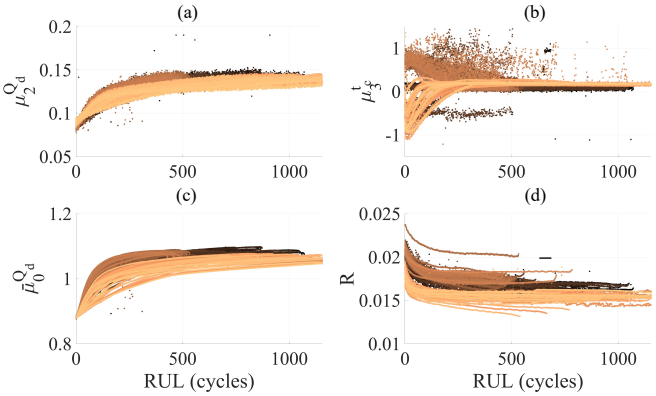

Fig. 6: Correlation between the RUL and selected features. (a) the variance of used capacity during discharge vs. RUL. (b) the skewness of charge time vs. RUL. (c) the maximum used capacity during discharge vs. RUL. (d) the internal resistance vs. RUL. Each color indicates one cell.

Based on the feature importance analysis, we consider three additional scenarios where only current and voltage sensors

TABLE I: Comparison of the inputs and RUL prediction performance of different random forest models (model inputs are in the summary statistics format as discussed in Section III-A; the model-b and the model-f both are reported twice in the table for easier comparison purposes)

			Part A				Part B					Part C					
			a	b	c	d	b	e	f	g	h	f	i	j	k	l	m
Model Inputs	Present charge cycle	Duration	✓	✓	✓		✓	✓	✓	✓	✓	✓	✓	✓	✓	✓	✓
		Used capacity	✓	✓	✓		✓	✓	✓	✓	✓	✓	✓	✓	✓	✓	✓
		Voltage	✓	✓	✓		✓	✓	✓	✓	✓	✓	✓	✓	✓	✓	✓
		Temperature	✓														
		Resistance	✓														
	Present discharge cycle	Duration	✓	✓		✓	✓	✓	✓	✓	✓	✓	✓	✓	✓	✓	✓
		Used capacity	✓	✓		✓	✓	✓	✓	✓	✓	✓	✓	✓	✓	✓	✓
		Voltage	✓	✓		✓	✓	✓	✓	✓	✓	✓	✓	✓	✓	✓	✓
		Temperature	✓														
		Resistance	✓														
SOC Range	SOC_{init}		0	0	0	0	0	0.1	0.2	0.3	0.4	0.2	0.2	0.2	0.2	0.2	0.2
	SOC_{end}		1	1	1	1	1	0.9	0.8	0.7	0.6	0.8	0.8	0.8	0.8	0.8	0.8
	SOC_{init} uncertainty		0	0	0	0	0	0	0	0	0	0	$\frac{1}{300}$	$\frac{1}{100}$	$\frac{2}{100}$	$\frac{1}{300}$	$\frac{1}{300}$
	SOC_{end} uncertainty		0	0	0	0	0	0	0	0	0	0	$\frac{1}{300}$	$\frac{1}{100}$	$\frac{2}{100}$	$\frac{1}{100}$	$\frac{2}{100}$
RUL prediction Mean Absolute Error (cycle)			62	62	74	95	62	64	67	71	85	67	68	74	84	70	74

are required (summarized in Part A of Table I): i) using features from t_c, t_d, V_c, V_d, Q_c, and Q_d (model-b); ii) using features from t_c, V_c, and Q_c (model-c); iii) using features from t_d, V_d, and Q_d (model-d). The RUL prediction performance of the above scenarios (i.e., by training and evaluating a model for each scenario) is also summarized at the bottom row of Table I. Consistent with Observation 3, the prediction accuracy is barely affected by removing the temperature and internal resistance-related features. However, the performance considerably deteriorates if only the charge or discharge data is utilized. A larger prediction error occurs when the charge data has been left out of the RUL prediction, matching with Observation 2 and the discussion based on Fig. 6. According to the performance in Part A of Table I, we then consider only using the features from t_c, t_d, V_c, V_d, Q_c, and Q_d (i.e., voltage and current sensors) in the subsequent development and analysis.

IV. RUL PREDICTION UNDER PARTIAL CHARGE & DISCHARGE

This section investigates the RUL prediction under partial charge and discharge conditions. First, the prediction performance under different partial charge and discharge ranges with perfect knowledge of SOC is presented. Then, the effect of uncertainties in the SOC information on the RUL prediction performance is studied.

A. Partial charge & discharge with accurate SOC information

The analysis in Section III shows that RUL prediction may be achieved with the charge and discharge data of a complete aging cycle. However, completely discharging or fully charging a cell seldom happens in many applications (e.g., EV applications) due to safety considerations or user patterns. Therefore, RUL prediction under partial charge and discharge conditions must be studied for an approach feasible in realistic conditions.

Although a few battery degradation datasets collected under partial charge and discharge are publicly available, these datasets only contain a limited number of cells, and the cells in the dataset may not be sufficiently aged (e.g., to 80% nominal capacity). Therefore, in this study, we create partial charge and discharge datasets truncated from the complete charge and discharge cycle data presented in Section II. In particular, t_j, Q_j, and V_j profiles ($j = c, d$) will be truncated based on the selected initial and end SOC values denoted as SOC_{ini} and SOC_{end}, respectively. After the truncation, t_c and Q_c will be

indexed from zero when cell SOC reaches SOC_{ini}, and t_d and Q_d will be indexed from zero when cell SOC reaches SOC_{end}. See Fig. 7 for an illustration of the data truncation.

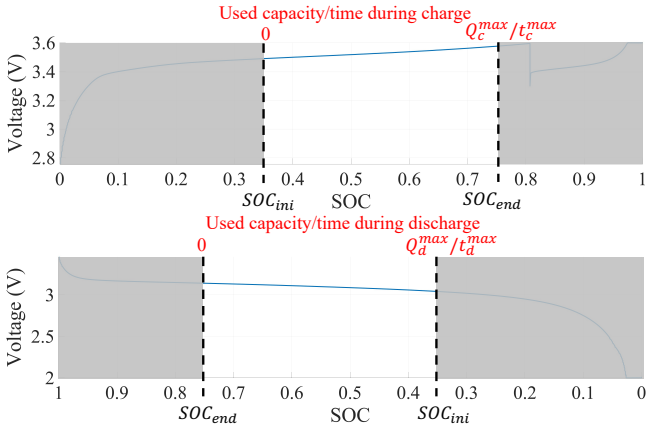

Fig. 7: Partial charge and discharge curves

Following the above truncation procedure, we consider the scenario where the initial and end SOC values are the same for all cells across different cycles. This corresponds to a scenario where the RUL prediction will be activated once the cell operates within a designated SOC range, completing a specified charge and discharge protocol, and accurate knowledge of the SOC is available. Five different designated SOC ranges are considered (summarized in Part B of Table I): i) SOC $\in [0, 1]$ (model-b, reused from Part A), ii) SOC $\in [0.1, 0.9]$ (model-e), iii) SOC $\in [0.2, 0.8]$ (model-f), iv) SOC $\in [0.3, 0.7]$ (model-g), and v) SOC $\in [0.4, 0.6]$ (model-h). The random forest is applied to the dataset created under each designated SOC range (to develop a model and evaluate it), and the performance is summarized in the last row of Part B in Table I. The RUL prediction performance will degrade as the SOC range decreases since less information will be available. However, it is noteworthy that when the SOC range is reduced to $[0.2, 0.8]$, which is the typical operating range for EVs, the RUL prediction performance is only reduced by 5 cycles in MAE compared to the performance achieved with complete charge and discharge cycles.

B. Partial charge & discharge with uncertain SOC information

Considering that the SOC can not be directly measured using sensors during battery operation, SOC typically has to be estimated for onboard applications. Consequently, the SOC information will inevitably contain uncertainties. To investigate the prediction performance under realistic scenarios, we focus on the RUL prediction using data collected over the SOC range of $[0.2, 0.8]$. Meanwhile, to account for the uncertainty in SOC, we perform data truncation with the actual initial (SOC^a_{ini}) and end SOC (SOC^a_{end}) values sampled from $\mathcal{N}(0.2, \sigma^2_{ini})$ and $\mathcal{N}(0.8, \sigma^2_{end})$ respectively, where $\mathcal{N}(\mu, \sigma^2)$ denotes a normal distribution with mean μ and standard deviation σ.

Based on the SOC estimation accuracy reported in [44], [45], we first examine the RUL prediction performance when $\sigma_{ini} = \sigma_{end}$ and the standard deviation values are 0.00333, 0.01, or 0.02. According to the three-sigma limits, these four standard deviation setups represent the scenarios when the maximum SOC estimation error is about 1%, 3%, or 6%, respectively. The MAE is listed in Part C of Table I along with the model setup. It can be seen that when the standard deviation is above 0.01, the RUL prediction error increases significantly. Considering that the SOC estimation error can be up to 5%, the proposed approach may have compromised performance in real-world applications.

Although the maximum SOC estimation error can be up to 5%, it mostly happens in the region where the open-circuit voltage (OCV) and SOC relationship is nearly flat (i.e., the OCV-SOC slope is close to zero). For LFP cells, the OCV-SOC plateau includes the region where SOC is near 0.8 but may not include the region where SOC is near 0.2 [46]. Therefore, the SOC estimation error at SOC near 0.2 can be overestimated above. We then further examine the RUL prediction performance when $\sigma_{ini} = 0.00333$, and σ_{end} can be 0.01 or 0.02. From Part C in Table I, we see that the RUL prediction performance is minimally affected by the increase in uncertainty in SOC^a_{end}, indicating that the RUL-related features located near SOC = 0.2 are important. The RUL prediction performance on different cells in the testing data with $\sigma_{ini} = 0.00333$ and $\sigma_{end} = 0.02$ (i.e., model-m) is also provided in Fig. 8, which shows that the RUL prediction accuracy can improve as the cell approaches its EOL.

V. Performance Evaluation

In this section, we first compare the proposed approach with a CNN-based RUL prediction approach to demonstrate its effectiveness. Then, sensitivity analysis is performed to understand the contribution of information from different SOC intervals to RUL prediction. Finally, extensive validation on different temperatures, C rates, and cell chemistry is conducted with another open-source dataset.

A. Comparison to a CNN-based approach

The performance of a CNN-based approach that directly uses four aging cycles (i.e., no extraction of statistical features) under complete charge and discharge, including t_j, V_j, I_j, and T_j $(j = c, d)$, presented in [26] is adopted for the comparison. We compare it with the performance of the random forest models using t_j, Q_j, and V_j $(j = c, d)$ under the following settings:

1) One aging cycle under complete charge and discharge, i.e., model-b in Table I;
2) One aging cycle under SOC $\in [0.2, 0.8]$ with $\sigma_{ini} = \sigma_{end} = 0$, i.e., model-f in Table I;
3) One aging cycle under SOC $\in [0.2, 0.8]$ with $\sigma_{ini} = 0.00333$, $\sigma_{end} = 0.02$, i.e., model-m in Table I.

The MAE is reported in Table II. When the data of complete charge and discharge is available, less degradation data/history of the target cell is required by the proposed approach, i.e., no need for temperature measurements and only one aging cycle data needed. Moreover, the proposed approach can achieve better prediction accuracy, i.e., a 3 cycle improvement in

This article has been accepted for publication in IEEE Transactions on Transportation Electrification. This is the author's version which has not been fully edited and content may change prior to final publication. Citation information: DOI 10.1109/TTE.2023.3323976

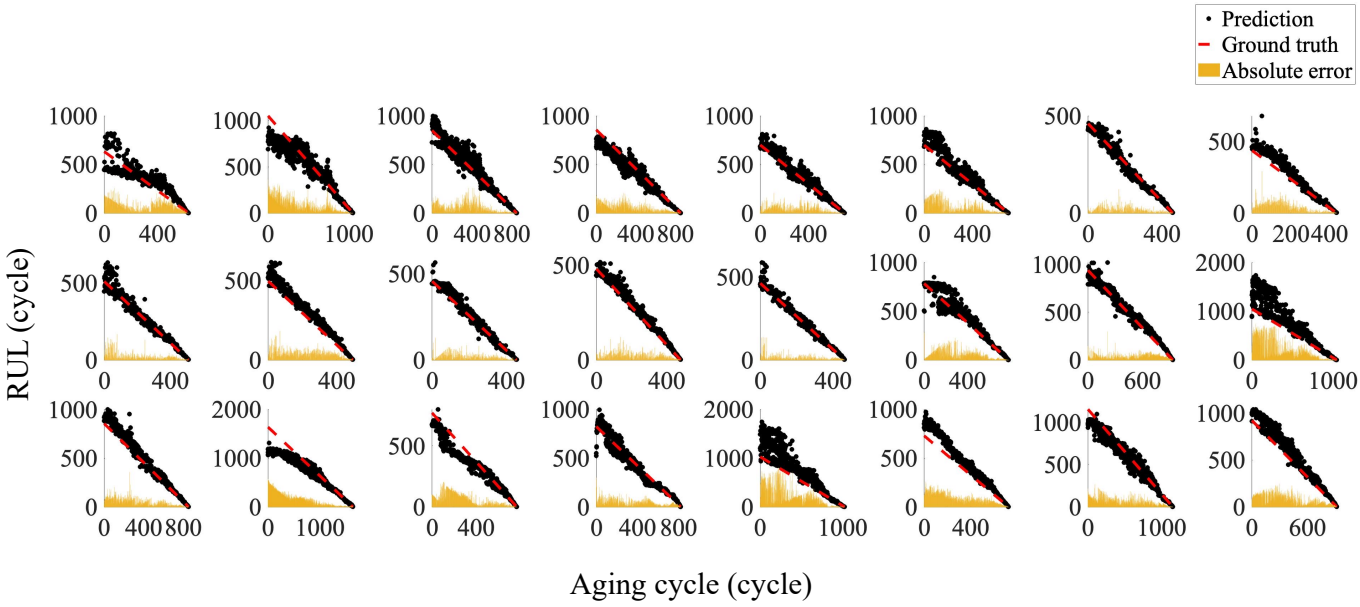

Fig. 8: RUL predictions, ground truth RUL, and absolute RUL prediction error over aging cycles across the cells in the testing data from [31] under SOC range of [0.2, 0.8] (model-m in Table I using features from $t_c, t_d, V_c, V_d, Q_c, Q_d$; $\sigma_{ini} = 0.00333$, $\sigma_{end} = 0.02$; each subplot contains the results for a different cell)

TABLE II: RUL prediction performance comparison with the existing approach

	MAE (cycle)
CNN: four full cycles [26] ($t_c, t_d, V_c, V_d, I_c, I_d, T_c, T_d$; SOC $\in [0, 1]$, $\sigma_{ini} = 0$, $\sigma_{end} = 0$)	65
Random forest (Model-b in Table I): one full cycle ($t_c, t_d, V_c, V_d, Q_c, Q_d$; SOC $\in [0, 1]$, $\sigma_{ini} = 0$, $\sigma_{end} = 0$)	62
Random forest (Model-f in Table I): partial cycle ($t_c, t_d, V_c, V_d, Q_c, Q_d$; SOC $\in [0.2, 0.8]$, $\sigma_{ini} = 0$, $\sigma_{end} = 0$)	67
Random forest (Model-m in Table I): partial cycle ($t_c, t_d, V_c, V_d, Q_c, Q_d$; SOC $\in [0.2, 0.8]$, $\sigma_{ini} = 1/300$, $\sigma_{end} = 0.02$)	74

MAE. This is primarily because the important signals are identified from feature importance analysis, thereby avoiding the overfitting issue during the model training and improving the generalizability of the machine learning model. When only partial charge and discharge are allowed, the proposed approach can still provide RUL prediction in the presence of uncertainties in SOC with merely a 9 cycle deterioration in MAE compared to the CNN-based approach.

B. Importance of the features from different SOC intervals

The above studies mostly focus on the RUL prediction performance under SOC ranges representing typical EV operations. In real-world applications, users may want to design specific protocols with different choices of the operating SOC range to balance the RUL prediction accuracy and user experience. To facilitate choosing the ideal SOC range, a sensitivity analysis is performed based on the partial cycle truncation procedure discussed in Section IV-A. Assuming perfect knowledge of SOC, datasets containing the partial cycle from SOC range of $[SOC_s, SOC_s + 0.1]$ for $SOC_s = 0.1, 0.2, ..., 0.8$ are created. By training random forest using these datasets, the RUL prediction accuracy is summarized in Table III, showing that the predictability of the data in different SOC intervals varies, and the data in the SOC interval of $[0.1, 0.2]$ contains the richest information for RUL prediction. This is the nonlinear region in the OCV-SOC curve, where the slope of the OCV-SOC curve is larger for LFP cells, indicating active lithium intercalation process [47]. Consequently, a good detectability of battery internal states (e.g., SOC and SOH) and degradation mode typically exists in this region [48],

TABLE III: RUL prediction performance using the features from $t_c, t_d, V_c, V_d, Q_c, Q_d$ under different SOC intervals

SOC Range	0.0 - 1.0	0.1 - 0.2	0.2 - 0.3	0.3 - 0.4	0.4 - 0.5	0.5 - 0.6	0.6 - 0.7	0.7 - 0.8	0.8 - 0.9
MAE (cycle)	62	69	72	78	86	88	91	89	89

TABLE IV: Extensive validation under the dataset in [49] (charge @ 0.5C and discharge @ 1C; cell nominal capacity 3.5 Ah)

Chemistry	Temperature	MAE (cycle)		
		One full cycle: SOC $\in [0,1]$ $\sigma_{ini}=0$, $\sigma_{end}=0$	partial cycle: SOC $\in [0.2,0.8]$ $\sigma_{ini}=0$, $\sigma_{end}=0$	partial cycle: SOC $\in [0.2,0.8]$ $\sigma_{ini}=1/300$, $\sigma_{end}=0.02$
NCM	45 C	7	8	12
NCA	45 C	21	21	28
	25 C	12	12	15

facilitating better RUL prediction accuracy.

C. Extensive validation under different temperatures, C rates, and battery chemistry

To further demonstrate the robustness of the proposed approach, we adopt the dataset provided in [49]. The dataset contains 18650-type batteries of different chemistry (i.e., NCM and NCA) tested under repeated aging cycles in a temperature-controlled chamber at $25, 35,$ or 45 C. During cycling, the charge and discharge C rates are the same for each cell but may vary across cells (from 0.25 C to 4 C). To ensure a sufficient number of cells with enough degradation (i.e., 80% of nominal capacity) for the RUL prediction study, we consider data under the following three scenarios, where the cell nominal capacity is 3.5 Ah, and the charge and discharge rate are 0.5 and 1 C, respectively:

1) NCM battery under 45 C ambient temperature with cutoff voltage 2.5-4.2 V;
2) NCA battery under 45 C ambient temperature with cutoff voltage 2.65-4.2 V;
3) NCA battery under 25 C ambient temperature with cutoff voltage 2.65-4.2 V.

By training a random forest model and evaluating it in each scenario, the RUL prediction performance under complete or partial cycles is then reported in Table IV for the three scenarios. It can be seen that satisfactory RUL prediction performance can be achieved under realistic SOC operating ranges regardless of the cell chemistry and ambient temperature. Meanwhile, since the C rate from this dataset differs from the one used in Section V-A, the effectiveness of the proposed approach under different C rates can also be demonstrated. Fig. 9 illustrates the RUL prediction performance under partial cycles with SOC uncertainties for the three scenarios, showing that reasonable RUL predictions can be obtained at different aging conditions of a cell.

VI. Conclusions and Future Work

In this work, the random forest technique is adopted to investigate the RUL prediction of lithium-ion battery cells. To probe the least amount of data required for RUL prediction, random forest models are developed using a fast-charging and discharging dataset, and the importance of the input features is quantitatively analyzed. The analysis reveals that the information on duration, used capacity, and voltage collected under both charge and discharge is required to ensure satisfactory RUL prediction accuracy. To verify the effectiveness of the proposed approach under realistic operations, the prediction performance under partial charge and discharge is also studied in the presence of uncertainties in the SOC. The prediction results indicate that satisfactory performance can be achieved with the RUL-related features in the SOC range of $[0.2, 0.8]$. Performance comparison with a CNN-based approach shows that the proposed approach renders better accuracy and requires less battery operating data. Extensive validation on other datasets demonstrates the robustness of the proposed approach under different cell chemistry, temperatures, and C rates.

In this study, instead of developing one model to handle the RUL prediction under arbitrary ambient temperatures and C rates, we propose to develop one random forest model for each operating condition. This is primarily due to a shortage in battery degradation data under a wide range of ambient temperatures/C rates, which can be costly to obtain. Therefore, in the future, we would like to explore leveraging physics-based degradation models/other data-driven models to augment the proposed approach for a unified model generic for different ambient temperatures/C rates. Moreover, investigating the RUL prediction of batteries in string/pack settings is also of interest. In this case, the problem is more challenging as it is subject to the impact of cell-to-cell variations and (likely uneven) cooling conditions.

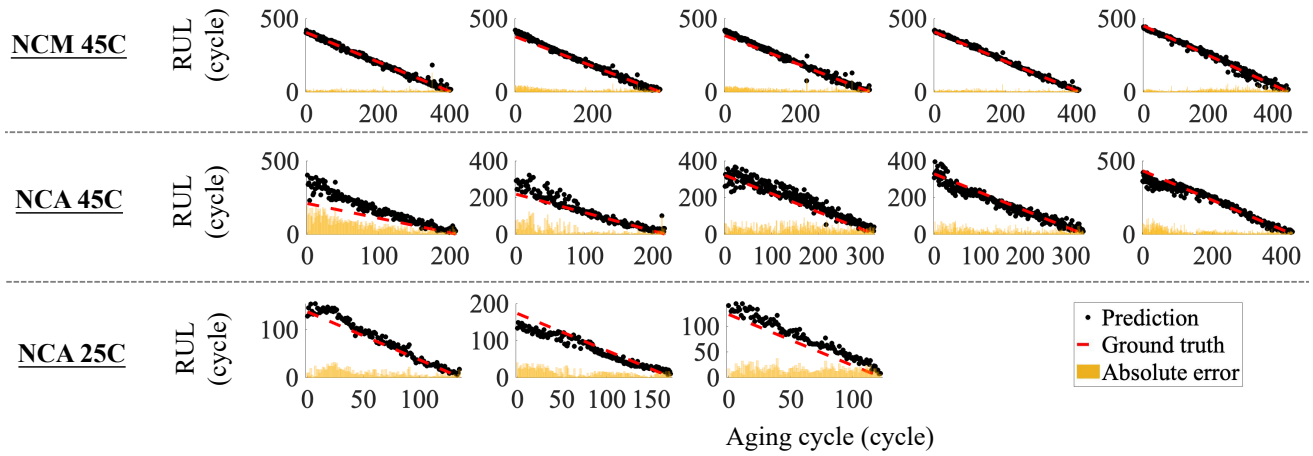

Fig. 9: RUL prediction, ground truth RUL, and absolute RUL prediction error over aging cycles across the cells in the testing data from [49] (models in Table IV using features from $t_c, t_d, V_c, V_d, Q_c, Q_d$; $\sigma_{ini} = 0.00333$, $\sigma_{end} = 0.02$; each subplot contains the results for a different cell)

REFERENCES

[1] A. Khaligh and Z. Li, "Battery, ultracapacitor, fuel cell, and hybrid energy storage systems for electric, hybrid electric, fuel cell, and plug-in hybrid electric vehicles: State of the art," *IEEE transactions on Vehicular Technology*, vol. 59, no. 6, pp. 2806–2814, 2010.

[2] Y. Liang, C.-Z. Zhao, H. Yuan, Y. Chen, W. Zhang, J.-Q. Huang, D. Yu, Y. Liu, M.-M. Titirici, Y.-L. Chueh *et al.*, "A review of rechargeable batteries for portable electronic devices," *InfoMat*, vol. 1, no. 1, pp. 6–32, 2019.

[3] Z. Miao, L. Xu, V. R. Disfani, and L. Fan, "An SOC-based battery management system for microgrids," *IEEE Transactions on Smart Grid*, vol. 5, no. 2, pp. 966–973, 2013.

[4] Y. Lei, N. Li, S. Gontarz, J. Lin, S. Radkowski, and J. Dybala, "A model-based method for remaining useful life prediction of machinery," *IEEE Transactions on Reliability*, vol. 65, no. 3, pp. 1314–1326, 2016.

[5] J. Li, S. He, Q. Yang, Z. Wei, Y. Li, and H. He, "A comprehensive review of second life batteries towards sustainable mechanisms: Potential, challenges, and future prospects," *IEEE Transactions on Transportation Electrification*, 2022.

[6] A. Theissler, J. Pérez-Velázquez, M. Kettelgerdes, and G. Elger, "Predictive maintenance enabled by machine learning: Use cases and challenges in the automotive industry," *Reliability Engineering & System Safety*, vol. 215, p. 107864, 2021.

[7] Z. Song, S. Feng, L. Zhang, Z. Hu, X. Hu, and R. Yao, "Economy analysis of second-life battery in wind power systems considering battery degradation in dynamic processes: Real case scenarios," *Applied Energy*, vol. 251, p. 113411, 2019.

[8] X. Han, L. Lu, Y. Zheng, X. Feng, Z. Li, J. Li, and M. Ouyang, "A review on the key issues of the lithium ion battery degradation among the whole life cycle," *ETransportation*, vol. 1, p. 100005, 2019.

[9] W. Gu and C. Wang, "Thermal-electrochemical modeling of battery systems," *Journal of The Electrochemical Society*, vol. 147, no. 8, p. 2910, 2000.

[10] X. Hu, H. Yuan, C. Zou, Z. Li, and L. Zhang, "Co-estimation of state of charge and state of health for lithium-ion batteries based on fractional-order calculus," *IEEE Transactions on Vehicular Technology*, vol. 67, no. 11, pp. 10 319–10 329, 2018.

[11] A. Bavand, S. A. Khajehoddin, M. Ardakani, and A. Tabesh, "Online estimations of li-ion battery SOC and SOH applicable to partial charge/discharge," *IEEE Transactions on Transportation Electrification*, vol. 8, no. 3, pp. 3673–3685, 2022.

[12] Y. Dahmane, R. Chenouard, M. Ghanes, and M. Alvarado-Ruiz, "Optimized time step for electric vehicle charging optimization considering cost and temperature," *Sustainable Energy, Grids and Networks*, vol. 26, p. 100468, 2021.

[13] C. Chen and M. Pecht, "Prognostics of lithium-ion batteries using model-based and data-driven methods," in *IEEE Prognostics and System Health Management Conference*, 2012, pp. 1–6.

[14] F. Yang, D. Wang, Y. Xing, and K.-L. Tsui, "Prognostics of li (NiMnCo) O2-based lithium-ion batteries using a novel battery degradation model," *Microelectronics Reliability*, vol. 70, pp. 70–78, 2017.

[15] X. Xu, S. Tang, C. Yu, J. Xie, X. Han, and M. Ouyang, "Remaining useful life prediction of lithium-ion batteries based on Wiener process under time-varying temperature condition," *Reliability Engineering & System Safety*, vol. 214, p. 107675, 2021.

[16] D. Wang, F. Yang, Y. Zhao, and K.-L. Tsui, "Battery remaining useful life prediction at different discharge rates," *Microelectronics Reliability*, vol. 78, pp. 212–219, 2017.

[17] W. He, N. Williard, M. Osterman, and M. Pecht, "Prognostics of lithium-ion batteries using extended Kalman filtering," in *IMAPS Advanced Technology Workshop on High Reliability Microelectronics for Military Applications*, vol. 1719, 2011.

[18] Z. Xue, Y. Zhang, C. Cheng, and G. Ma, "Remaining useful life prediction of lithium-ion batteries with adaptive unscented Kalman filter and optimized support vector regression," *Neurocomputing*, vol. 376, pp. 95–102, 2020.

[19] A. El Mejdoubi, H. Chaoui, H. Gualous, P. Van Den Bossche, N. Omar, and J. Van Mierlo, "Lithium-ion batteries health prognosis considering aging conditions," *IEEE Transactions on Power Electronics*, vol. 34, no. 7, pp. 6834–6844, 2018.

[20] Y. Li, K. Liu, A. M. Foley, A. Zülke, M. Berecibar, E. Nanini-Maury, J. Van Mierlo, and H. E. Hoster, "Data-driven health estimation and lifetime prediction of lithium-ion batteries: A review," *Renewable and Sustainable Energy Reviews*, vol. 113, p. 109254, 2019.

[21] J. Wei, G. Dong, and Z. Chen, "Remaining useful life prediction and state of health diagnosis for lithium-ion batteries using particle filter and support vector regression," *IEEE Transactions on Industrial Electronics*, vol. 65, no. 7, pp. 5634–5643, 2017.

[22] A. Thelen, M. Li, C. Hu, E. Bekyarova, S. Kalinin, and M. Sanghadasa, "Augmented model-based framework for battery remaining useful life prediction," *Applied Energy*, vol. 324, p. 119624, 2022.

[23] W. Qin, H. Lv, C. Liu, D. Nirmalya, and P. Jahanshahi, "Remaining useful life prediction for lithium-ion batteries using particle filter and artificial neural network," *Industrial Management & Data Systems*, vol. 120, no. 2, pp. 312–328, 2020.

[24] S. Zhao, C. Zhang, and Y. Wang, "Lithium-ion battery capacity and remaining useful life prediction using board learning system and long short-term memory neural network," *Journal of Energy Storage*, vol. 52, p. 104901, 2022.

[25] J. Zhang, Y. Jiang, S. Wu, X. Li, H. Luo, and S. Yin, "Prediction of remaining useful life based on bidirectional gated recurrent unit with temporal self-attention mechanism," *Reliability Engineering & System Safety*, vol. 221, p. 108297, 2022.

[26] J. Hong, D. Lee, E.-R. Jeong, and Y. Yi, "Towards the swift prediction of the remaining useful life of lithium-ion batteries with end-to-end deep learning," *Applied Energy*, vol. 278, p. 115646, 2020.

[27] C. Strange and G. Dos Reis, "Prediction of future capacity and internal

resistance of li-ion cells from one cycle of input data," *Energy and AI*, vol. 5, p. 100097, 2021.
[28] J. Lu, R. Xiong, J. Tian, C. Wang, C.-W. Hsu, N.-T. Tsou, F. Sun, and J. Li, "Battery degradation prediction against uncertain future conditions with recurrent neural network enabled deep learning," *Energy Storage Materials*, vol. 50, pp. 139–151, 2022.
[29] L. Breiman, "Random forests," *Machine learning*, vol. 45, no. 1, pp. 5–32, 2001.
[30] U. Grömping, "Variable importance assessment in regression: linear regression versus random forest," *The American Statistician*, vol. 63, no. 4, pp. 308–319, 2009.
[31] K. A. Severson, P. M. Attia, N. Jin, N. Perkins, B. Jiang, Z. Yang, M. H. Chen, M. Aykol, P. K. Herring, D. Fraggedakis *et al.*, "Data-driven prediction of battery cycle life before capacity degradation," *Nature Energy*, vol. 4, no. 5, pp. 383–391, 2019.
[32] S. Saxena, C. Le Floch, J. MacDonald, and S. Moura, "Quantifying EV battery end-of-life through analysis of travel needs with vehicle powertrain models," *Journal of Power Sources*, vol. 282, pp. 265–276, 2015.
[33] L. C. Casals, B. A. García, and C. Canal, "Second life batteries lifespan: Rest of useful life and environmental analysis," *Journal of Environmental Management*, vol. 232, pp. 354–363, 2019.
[34] X.-G. Yang, Y. Leng, G. Zhang, S. Ge, and C.-Y. Wang, "Modeling of lithium plating induced aging of lithium-ion batteries: Transition from linear to nonlinear aging," *Journal of Power Sources*, vol. 360, pp. 28–40, 2017.
[35] P. Fermín-Cueto, E. McTurk, M. Allerhand, E. Medina-Lopez, M. F. Anjos, J. Sylvester, and G. Dos Reis, "Identification and machine learning prediction of knee-point and knee-onset in capacity degradation curves of lithium-ion cells," *Energy and AI*, vol. 1, p. 100006, 2020.
[36] C. Weng, Y. Cui, J. Sun, and H. Peng, "On-board state of health monitoring of lithium-ion batteries using incremental capacity analysis with support vector regression," *Journal of Power Sources*, vol. 235, pp. 36–44, 2013.
[37] N. Yang, Z. Song, H. Hofmann, and J. Sun, "Robust state of health estimation of lithium-ion batteries using convolutional neural network and random forest," *Journal of Energy Storage*, vol. 48, p. 103857, 2022.
[38] X. Hu, L. Xu, X. Lin, and M. Pecht, "Battery lifetime prognostics," *Joule*, vol. 4, no. 2, pp. 310–346, 2020.
[39] V. Y. Kulkarni and P. K. Sinha, "Pruning of random forest classifiers: A survey and future directions," in *IEEE International Conference on Data Science & Engineering*, 2012, pp. 64–68.
[40] F. Pedregosa, G. Varoquaux, A. Gramfort, V. Michel, B. Thirion, O. Grisel, M. Blondel, P. Prettenhofer, R. Weiss, V. Dubourg *et al.*, "Scikit-learn: Machine learning in python," *Journal of Machine Learning Research*, vol. 12, pp. 2825–2830, 2011.
[41] A. Altmann, L. Toloşi, O. Sander, and T. Lengauer, "Permutation importance: a corrected feature importance measure," *Bioinformatics*, vol. 26, no. 10, pp. 1340–1347, 2010.
[42] J. Xu, H. Wang, H. Shi, and X. Mei, "Multi-scale short circuit resistance estimation method for series connected battery strings," *Energy*, vol. 202, p. 117647, 2020.
[43] L. Chen, Z. Lü, W. Lin, J. Li, and H. Pan, "A new state-of-health estimation method for lithium-ion batteries through the intrinsic relationship between ohmic internal resistance and capacity," *Measurement*, vol. 116, pp. 586–595, 2018.
[44] C. Liu, W. Liu, L. Wang, G. Hu, L. Ma, and B. Ren, "A new method of modeling and state of charge estimation of the battery," *Journal of Power Sources*, vol. 320, pp. 1–12, 2016.
[45] X. Lin, "Theoretical analysis of battery SOC estimation errors under sensor bias and variance," *IEEE Transactions on Industrial Electronics*, vol. 65, no. 9, pp. 7138–7148, 2018.
[46] R. Xiong, Q. Yu, C. Lin *et al.*, "A novel method to obtain the open circuit voltage for the state of charge of lithium ion batteries in electric vehicles by using H infinity filter," *Applied Energy*, vol. 207, pp. 346–353, 2017.
[47] T. Kalogiannis, D. I. Stroe, J. Nyborg, K. Nørregaard, A. E. Christensen, and E. Schaltz, "Incremental capacity analysis of a lithium-ion battery pack for different charging rates," *ECS Transactions*, vol. 77, no. 11, p. 403, 2017.
[48] Z. Song, X. Wu, X. Li, J. Sun, H. F. Hofmann, and J. Hou, "Current profile optimization for combined state of charge and state of health estimation of lithium ion battery based on Cramer–Rao bound analysis," *IEEE Transactions on Power Electronics*, vol. 34, no. 7, pp. 7067–7078, 2018.
[49] J. Zhu, Y. Wang, Y. Huang, R. Bhushan Gopaluni, Y. Cao, M. Heere, M. J. Mühlbauer, L. Mereacre, H. Dai, X. Liu *et al.*, "Data-driven capacity estimation of commercial lithium-ion batteries from voltage relaxation," *Nature Communications*, vol. 13, no. 1, p. 2261, 2022.

Niankai Yang received the B.E. degree from Shanghai Jiao Tong University, Shanghai, China in 2016 and Ph.D. degree from the University of Michigan, Ann Arbor, MI, USA in 2022, all in naval architecture and marine engineering. His current research interests include machine learning for condition monitoring of lithium-ion batteries, model predictive control and its application, and planning and control of autonomous vehicles.

Heath Hofmann (Fellow, IEEE) received the Ph.D. degree in electrical engineering and computer science from the University of California at Berkeley, Berkeley, CA, USA, in 1998. He is currently a Professor with the University of Michigan, Ann Arbor, MI, USA. He has authored approximately four dozen papers in refereed journals. He currently holds 14 patents. His research interests include power electronics, specializing in the design, simulation, and control of electromechanical systems, adaptive control techniques, energy harvesting, flywheel energy storage systems, electric and hybrid electric vehicles, and finite-element analysis.

Jing Sun (Fellow, IEEE) received the Ph.D. degree from the University of Southern California, Los Angeles, CA, USA in 1989. She is currently the Michael G. Parsons Collegiate Professor with the Department of Naval Architecture and Marine Engineering, with joint appointments at the Department of Electrical Engineering and Computer Science, and the Department of Mechanical Engineering, University of Michigan, Ann Arbor, MI, USA. Her research interests include modeling, control, and optimization of dynamic systems, with applications to marine and automotive systems. She is a fellow of the National Academy of Inventors, IFAC (International Federation of Automatic Control), and the Society of Naval Architects and Marine Engineers. She was a recipient of the 2003 IEEE Control System Technology Award.

Ziyou Song (Senior Member, IEEE) is an Assistant Professor at the Department of Mechanical Engineering at the National University of Singapore. He received his B.E. degree (with honours) and Ph.D. degree (with highest honours) in Automotive Engineering from Tsinghua University, Beijing, China, in 2011 and 2016, respectively. Dr. Song's research interests lie in the areas of modeling, estimation, optimization, and control of energy storage (e.g., battery, supercapacitor, and flywheel) for electrified vehicles and renewable energy systems. Using energy storage as a bridge, his group is actively connecting the automotive, transportation, and power system communities by collaborating on interdisciplinary projects.